Data-analysis and modelling of the effect of inter-row shading on the power production of photovoltaic plants

Yves-Marie Saint-Drenan, Thibaut Barbier

Data-analysis and modelling of the effect of inter-row shading on the power production of photovoltaic plants

Yves-Marie Saint-Drenan [*1] and Thibaut Barbier[†1]

[1]MINES ParisTech, PSL Research University, O.I.E. Centre Observation, Impacts, Energy, 06904 Sophia Antipolis, France

March 2019

Abstract

The aim of this work is to propose a fast and easily implementable model allowing the consideration of inter-row shading in the simulation of the power production of PV plants. Our objective is to find the simplest model with the least number of input parameters. A formulation of the shaded fraction of the module area dependent on the PV configuration and the sun position is first proposed. An analysis of the measurements of two plants is then carried out to understand the effect of inter-row shading for a complete PV array. Based on this analysis, a model is proposed and validated. It is shown that the consideration of inter-row shading with the proposed model allows a relative improvement of the simulation accuracy (RMSE) ranging between 18 and 32 % for time steps affected by inter-row shading and between 7 and 12 % for a complete year.

Keyword : photovoltaic plants, power production simulation, field measurements, inter row shading

[*]yves-marie.saint-drenan@mines-paristech.fr
[†]thibaut.barbier@mines-paristech.fr

Nomenclature	
$\lceil \quad \rceil$	Ceiling function
α_P	Module azimuth angle [°]
α_s	Sun azimuth angle [°]
γ_P	Module tilt angle [°]
γ_s	Sun elevation angle [°]
γ_{shdg}	Shading angle [°]
μ_{temp}	Shading angle [°]
f_{inv}	Power curve of the inverter
$f_{mod,T=25°C}$	Power curve of the module for module temperature of 25°C
f_{PV}	Power curve of the PV plant
$f_{shading}$	Shaded fraction of the module area
GHI	Global horizontal irradiance [W/m^2]
G_{POA}	Plane of array irradiance [W/m^2]
H	Panel height [m]
IV	Current-Voltage
L	Pannel length [m]
MAE	Mean absolute error
N_p	Number of parallel strings
N_s	Number of cells connected in series along the vertical
P_{peak}	Peak power of the PV plant [W]
P_{PV}	Output PV power [W]
$P_{unshaded}$	Fully unshaded power production [W]
P_{shaded}	Fully shaded power production [W]
POA	Plane of array
PV	Photovoltaic
RMSE	Root mean square error
s	Row spacing [m]
string	set of PV panels connected together in series
T_{mod}	Module temperature [°C]
w	Weight factor
$w_{FullyShaded}$	Weight factor accounting for all strings fully shaded
$w_{PartiallyShaded}$	Weight factor accounting for the string partially shaded

1 Introduction

1.1 Motivation

Losses of energy production resulting from inter-row shading is unavoidable in rack mounted photovoltaic (PV) plants. A sufficient inter-row spacing must be planned in order to limit shading of a module row on another. It is however not rare to find plants where the spacing between rows is so small that yield losses due to row-to-row shading effects are significant. Such configurations result from low module prices and high ground costs: the maximum energy production per available ground area is pursued instead of the optimum energy production per peak power [5]. In such cases, an accurate consideration of the effect of inter-row shading on the power production is essential for any applications where the plant power output needs to be estimated (power monitoring, power forecast...).

During the planning phase of a solar plant, the effect of shading on the expected yield is considered very accurately using dedicated software like e.g. [11], [19] or [20]. With those tools, the shadow is calculated using three-dimensional geometrical calculations and its impact on the power assessed by combining IV curves of the different cells under consideration of their individual insolation as well as their interconnection. State-of-the-art models are used and the estimation is very accurate. This good performances are however reached at the expense of high computation time and it requires knowing a lot of detailed information on the plant.

There are various applications in which the output power generation of a PV plants needs to be estimated in real-time or near real-time (yield monitoring, power forecast...). In those applications, the best estimate of the plant power generation is searched but the calculation procedure is subjected to several constraints. Firstly, the available time and resource for estimating the power generation is limited so that the calculation needs to be fast and simple. Secondly, it is frequent that power calculation has to be conducted for plants for which little information is available. Using the detailed method of the above-mentioned commercial solutions is therefore excluded and a lighter alternative method is needed. In this paper, we propose a method for evaluating the impact of shading on the power production that matches the constraints of an online application, i.e. a simple and fast calculation method requiring the minimal amount of information on the plant.

1.2 Literature review

The development of models for considering the effect of partial shading on the PV power production started in the 1960s with the works of e.g. [14], [1], or [22] and is still an active field of research (see e.g. [25, 2]). As mentioned by [6], in most of these contributions, the authors calculate the effect of partial shading on the PV power generation by summing the forward and reverse current-voltage (IV) characteristics of the shaded and unshaded cells, providing the ability to simulate accurately an arbitrary shading condition and array configuration. [6] mention additionally that, "*computation speed is sacrificed to achieve this accuracy, and using a linear approach to simulate a large PV installation with thousands of panels and hundreds of thousands of individual cells requires long simulation times, with computation time scaling linearly with PV installation size.*" This computation costs explains that the increase of speed and calculation capacity of computers has brought about a growth of the number of research activities in this area (e.g. [4, 13, 21]). Some authors address directly the issue of the high computing costs by proposing calculation methods reducing the simulation time such as e.g. the Monte Carlo techniques used in [10]. Despite improvement of the computer capacity and increase of the calculation efficiency, the calculation time of these methods remain too long for applications needing fast yield estimations like e.g. failure detection or power forecast. For such applications, an accurate but simple and fast method is needed. Analytic models such as those proposed by [18], [16], [6] are designed to fill these requirements. A convenient feature of analytic models is also the reduced amount of information needed for the simulation compared to traditional approaches. However, collecting or estimating the plant information needed by those models can still represent an obstacle to their implementation. Indeed, when very limited amount of information is available on a plant, the determination of detailed plant characteristics such as series and shunt resistances [18], [10], number of blocks with bypass diodes [16], fill factor [6] is not obvious. The situation is frequent, where the power production of a PV plant has to be analyzed, estimated or forecasted, while this information is not available. If possible, a method using the minimal numbers of plant parameters while preserving the modeling accuracy would be desirable. Lastly, studies on partial shading are mostly focusing on the electrical aspect of the problem and the geometrical part is - to the best of our knowledge - rarely addressed. The only work providing a formula for the estimation of the shaded fraction is that proposed by [29] but it is limited to south-oriented PV plants with panels made of one single module row. This formulation is thus not general enough since many plants have an azimuth angle differing from the optimal south orientation

and PV arrays containing several module rows. A more general formulation of the shading fraction as a function of the geometrical characteristics of a plant would therefore be needed.

1.3 Contribution

The literature review above allowed identifying the need for a fast and simple analytic shading model which needs to have a minimal number of input parameters but a satisfying simulation accuracy. The present work aims to fill this gap by proposing a modelling approach pursuing this optimum. For this purpose, our model development is conducted in parallel to a data-analysis of power measurements from two large-scale PV plants that are affected by inter-row shading. This data-driven approach guarantees that our assumptions and modelling approach are of practical relevance and avoids considering parameters having a small effect on the power production. The ability of our modelling approach to be generalized to other plants is nevertheless also evaluated by testing the validity of our modelling assumptions using traditional IV curve summing simulations. In addition, we address the lack of calculation method for the estimation of the shaded fraction by proposing a formula for any plant configuration. The present papers address thus all calculation steps for the consideration of the effect of partial shading on the PV power calculation.

A description of the two PV plants considered in this work as well as all data used for the simulation and validation of the model is given in section 2. The analytic model development based on the data analysis is detailed in section 3. The resulting model is then validated against measurements in section 4 and conclusions on the present work are given in section 5.

2 Data description

2.1 PV plants and measurement dataset

The approach chosen in this paper consists in analyzing the effect of inter-row shading using measurement data as a motivation for the model validation and application conducted in section 3. Measurements from two PV plants - provided by Enerparc AG - are used for this purpose and are described in this section. Both PV plants are located in Eastern Germany. The main characteristics of the two plants are summarized in Table 1. They are located in Delitzsch and Althen and have a total peak capacity of $32 MW_p$ and $7 MW_p$ respectively. Both PV plants have a south orientation and a tilt angle of 25^o.

	Delitzsch	**Althen**
Latitude	51.50941^oN	51.345564^oN
Longitude	12.291311^oE	12.516578^oE
Total peak capacity	32091.84 kW_p	7347.60 kW_p
Number of inverters	37	11
Azimuth angle	180^o (South)	180^o (South)
Tilt Angle	25^o	25^o
Module orientation	landscape	landscape
Module width	0.99 m	0.99 m
Number of stacked panels along side of rows	4	4
Inter-row spacing	2.4 m	2.7 m
ID of the inverter analysed	INV_07_13	INV_04_07
Peak power of the inverter	1002.24 kW_p	750.12 kW_p

Table 1: Main characteristics and locations of the Delitzsch and Althen PV plants

The main geometrical characteristics of the two plants are given in Table 1. The meanings of the main parameters are illustrated in Figure 1. The panels are constituted of four rows of modules in landscape orientation. This layout can be observed in the aerial pictures of the plants in Figure 2. The inter-row spacing is equal to 2.4 and 2.7 m in Delitzsch and Althen respectively. These inter-row spacing values have been estimated on the basis of technical drawings of the plants. Even if there is some uncertainties on these values, they have been validated by the operators of the plants. An often-used metric to quantify the inter-row spacing with respect to the panel height and tilt angle consists in evaluating the shading angle, which is formed by the line joining the highest point of a panel with the lowest point of the following panel and the horizontal. This angle is illustrated in Figure 1. It is recommended to have a small value of the shading angle in order to avoid inter-row shading. A value of 14^o is for example recommended in [7], which corresponds to the maximal solar elevation at the winter solstice in Berlin. Using the tilt angles, inter-row spacing and panel length of the two plants, we found shading angle values of 35 and 32^o for Delitzsch and Althen respectively. These values are thus relatively high and indicate that important shading losses can be expected. The values of these angles have been confirmed by the plant operator and, as will be analyzed later, they are in line with the measurement analysis.

In both plants, the cells are interconnected according to a series-parallel concept: all PV modules of the panel row are connected together in series,

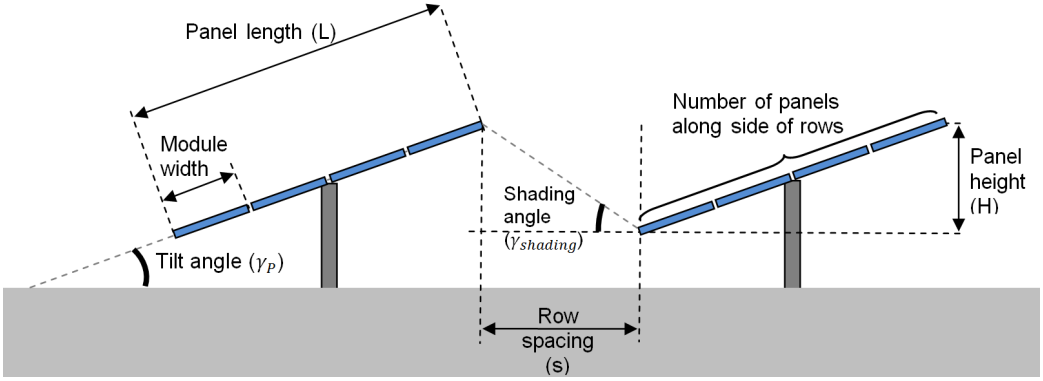

Figure 1: Definition of module row interspacing and the module height

which forms a string. In the two plants, a panel row is made of four different strings that are connected in parallel.

The dataset includes 1 min measurements of the output AC-power for each inverter of the two PV plants over a period comprised between 27/08/2012 and 31/01/2015 and between 01/05/2012 and 31/01/2015 for the plants located in Delitzsch and Althen respectively. For both plant, module temperature and plane-of-array irradiance measured by a reference cell are also available.

For the present analysis, we only used measurements of a single PV inverter, which is sufficient for our purpose and reduces significantly the size of the dataset. The inverters used for the analysis have been chosen, so that the corresponding PV arrays lay in the middle of the PV plant and is not affected by other shading than the inter-row shading (e.g. tree, building...). Information on the chosen inverters is provided in Table 1 and their spatial locations within the plants are illustrated in Figure 2.

2.2 Data needed for calculating the shading effect

The first step in modelling the effect of inter-row shading on the power production is the calculation of the shaded fraction of the PV panels. This is a geometrical calculation which requires the following information as input: the panel length L, the module orientation angles (α_P, γ_P), the inter-row spacing s and the solar position angles (α_s, γ_s). All these information are given in section 2.1 and the detail of the calculation of the shaded fraction are provided in section 3.2 as well as in A.

When a part of the modules is shaded, it is obvious that the direct radiation does not reach the shaded regions while the unshaded part of the modules benefits from all three components of the POA irradiation [16]. De-

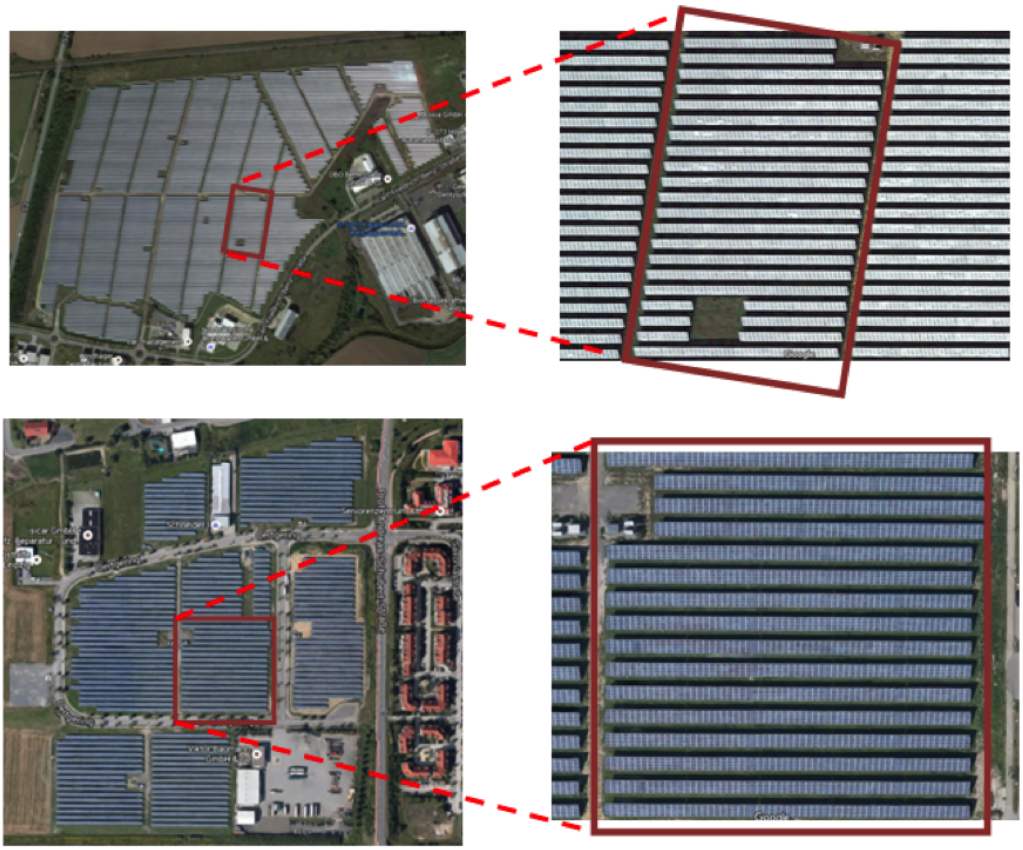

Figure 2: Aerial view of the Delitzsch and Althen PV plants: left: whole plant, right: array connected to the inverter, whose measurements are used in this analysis. (Source: Google earth)

pending on the level of shading, the PV power production will thus vary between the two following bounds:

- a lower value corresponding to power produced when only the diffuse and reflected radiation are received by the modules - the fully shaded power production P_{shaded}, and,
- an upper value corresponding to the power produced when all three components of the GHI are received by the modules - the fully unshaded power production $P_{unshaded}$.

As will be further explained in section 3, we propose a modelling approach in which the power production of a plant affected by shading is evaluated by a linear combination of these two power values. Their calculation is thus needed to simulate the effect of shading on the PV power. The calculation of

the power values corresponding to these two extreme situations is explained in the subsections 2.2.2 and 2.2.3. This preliminary step has been intentionally included in the section "data description" since any other methodology than that proposed below can be used for estimating these two simulated power values. The estimation of the shaded and unshaded power requires the knowledge of the three components of the irradiation whose evaluation is explained in the following subsection.

2.2.1 Estimation of the three components of the plane-of-array irradiation

Decomposition models - i.e. models allowing the estimation of the different components of the global irradiation - are usually developed for the global horizontal irradiation (GHI). Such measurements being not available at the two considered plants, two possibilities from the literature are possible: estimating the GHI from POA measurement [15, 8] or using satellite-derived GHI data. These two methods enable to decompose the POA and can be used in the proposed model. Both approaches having their respective strengths and weaknesses, we have chosen to use satellite-derived GHI data for its simplicity. The chosen data are taken from the HC3v5 database [9] and are 15-min time series of the global horizontal irradiation evaluated from MSG satellite images using the Heliosat-2 method [24]. Using satellite-derived GHI data, the direct and diffuse components of the horizontal irradiance have been estimated with the [27] decomposition model. The three components of the POA irradiance have then been calculated with the [17] transposition model. For this last step, a ground albedo of 20% has been assumed.

The sum of the three components of the POA irradiance estimated with the satellite data are plotted against the measured POA irradiance for the two plants in figure 3. It can be observed that satellite-based estimates of the POA irradiance generally match well with the corresponding measurements. A marked offset can however be observed for the PV plant located in Althen, which probably stems from a mismatch between the actual turbidity of the location and the climatologic value used in the calculation of Helioclim [23]. In addition, a relatively high dispersion of the scatter points can be observed, which is not surprising considering that 1-min point measurements are compared to timely interpolated values of spatial average irradiation (satellite pixel with an extension of several kilometres) available every 15 min.

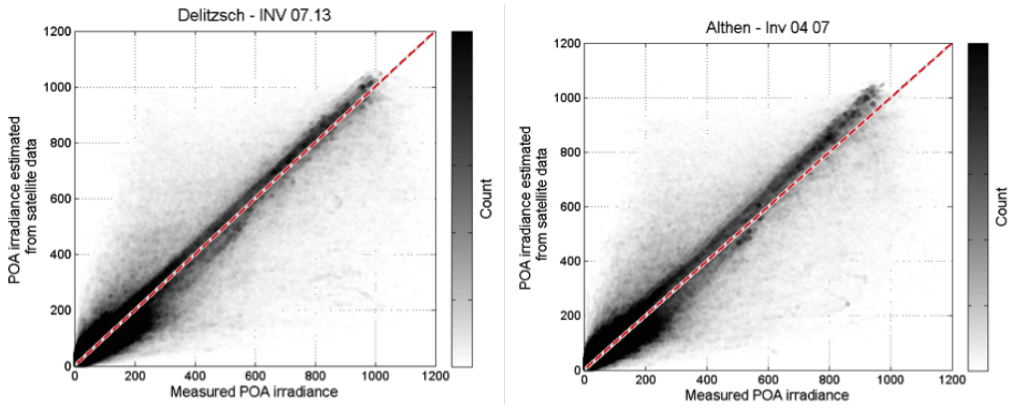

Figure 3: Scatter plot of the POA irradiance evaluated with the decomposition and transposition models on the basis of the satellite irradiance against the measured POA irradiance (left: Delitzsch, right: Althen)

2.2.2 Simulated power values corresponding to a fully unshaded condition

As previously mentioned, the potential power production $P_{unshaded}$ - that would have been realized without shading - needs to be estimated for the calculation of the effect of shading on the plant yield. In the following calculation, we assume that POA irradiation measurements are not affected by shading, which is in most situations the case. In order to calculate $P_{unshaded}$, a model giving the output power P_{PV} as a function of the measured POA irradiance G_{POA} and module temperature T_{mod} is needed.

A common approach for estimating the PV power production from temperature and irradiation measurements is to use the power curves of the inverter f_{inv} (e.g. [26]), the power curve of the module for a module temperature of 25^oC $f_{mod,T=25°C}$ and a temperature coefficient μ_{temp} (e.g. [3]). With this approach, the simulated PV power production P_{PV} can be expressed as a function of the two measured quantities T_{mod} and G_{POA} as follows:

$$P_{PV} = P_{peak} \times f_{inverter}(f_{mod,T=25°C}(G_{POA})) \times (1 + \mu_{temp} \times (T_{mod} - 25°C)) \quad (1)$$

A simple way of using the above equation consists in evaluating the functions $f_{inverter}$ and $f_{mod,T=25^oC}$ using information available on the module and inverter product-sheets. It is however not rare that actual module and inverter characteristics deviate from those expected from manufacturer information. This is why we prefer a more pragmatic approach consisting in inferring unknown plant parameters of the model from measurements. Estimating

the parameters of the model given in Eq. 1 is not easy since it is difficult to differentiate between the effects of the power curves of the inverter and module. The model was therefore simplified by introducing the power curve of the PV plant f_{PV}, which accounts for the aggregated effect of the module and inverter for a module temperature of 25^oC (f_{PV}=$f_{inverter} \circ f_{mod,T=25°C}$). The effect of the temperature is then considered with the AC power, which brings about a small modelling error. This error is however considered negligible considering the shape of most inverter power curves. With this simplification, the model can be expressed as follow:

$$P_{PV} \cong P_{peak} \times f_{PV}(G_{POA})) \times (1 + \mu_{temp} \times (T_{mod} - 25°C)) \qquad (2)$$

The power temperature coefficient μ_{temp} is assumed to be equal to $-0.4\%/^oC$ for the two PV plants. The function f_{PV} is then determined by a linear robust fit per interval using the temperature-corrected power and POA irradiance measurements. The temperature-corrected power data are represented as a function of the POA irradiance for the two plants in Figure 4. The assessed power curves are represented by red curves in Figure 4.

It can be observed in the two graphics of Figure 4 that the scatter points are organized in different lines crossing the origin. The upper line which includes most points correspond to a normal - shading-free - operation while the lower ones are resulting from the effect of shading on the operation of the modules. We are thus interested in evaluating a function that fits the upper line. As can be observed on the red curves in Figure 4, this is achieved thanks to the robust regression as long as the majority of the points are not affected by shading.

The time series of the power values $P_{unshaded}$ corresponding to a fully unshaded situation can thus be estimated on the basis of the POA irradiation and temperature measurements (G_{POA}, T_{mod}), using the estimated power curve f_{PV} and temperature coefficient μ_{temp}.

2.2.3 Simulated power values corresponding to a fully shaded condition

The calculation of the fully shaded power production P_{shaded} can be conducted using the approach presented in the last section whereby the direct POA irradiation is set equal to zero in order to take into account the effect of the shading. The diffuse and reflected POA irradiation evaluated with satellite data (see Section 2.2.1) are therefore summed and used for the calculation of the power values -P_{shaded}- corresponding to a fully shaded

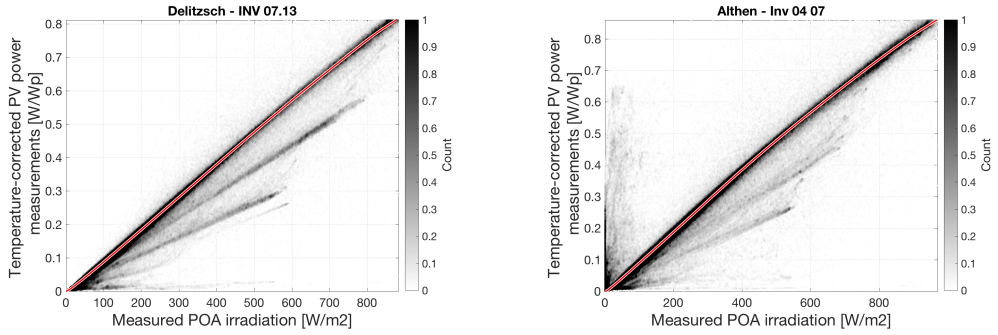

(a) Althen (b) Delitzsch

Figure 4: Temperature corrected power as a function of the POA irradiance (light grey to black dots) and estimated power curves (red curves).

situation using the function f_{PV} and temperature coefficient introduced in the previous section. The resulting power values are used in the following section for estimating the maximum power point (MPP) power production of a shaded PV system.

3 Modelling the effect of row-to-row shading on the PV-power production

This part describes the different steps in the modeling of row-to-row shading effect on the power production. The dataset presented in 2 is used as a motivation - or as a validation - of each step of the proposed model.

3.1 Overview of the modeling approach

While an accurate calculation of the maximum power production of an array affected by shading requires a detailed calculation of the IV curves, we propose a simpler approach consisting in a linear combination of the two extreme power values $P_{unshaded}$ and P_{shaded}. The respective influences of the two power values on the simulated output power P_{pv} are modulated by a weighting coefficient whose general form can be written:

$$P_{pv} = w \times P_{unshaded} + (1 - w) \times P_{shaded} \tag{3}$$

The weight factor w is a function of the shaded fraction of the panels and depends on the cell interconnection. A description of the calculation of the shaded fraction is first given in section 3.2. A data analysis of power measurements from our two large PV plants is then described in section 3.3, which is aimed at motivating the modelling approach explained in section 3.4. A flow chart illustrating the different steps and the corresponding equations is given in Figure 5.

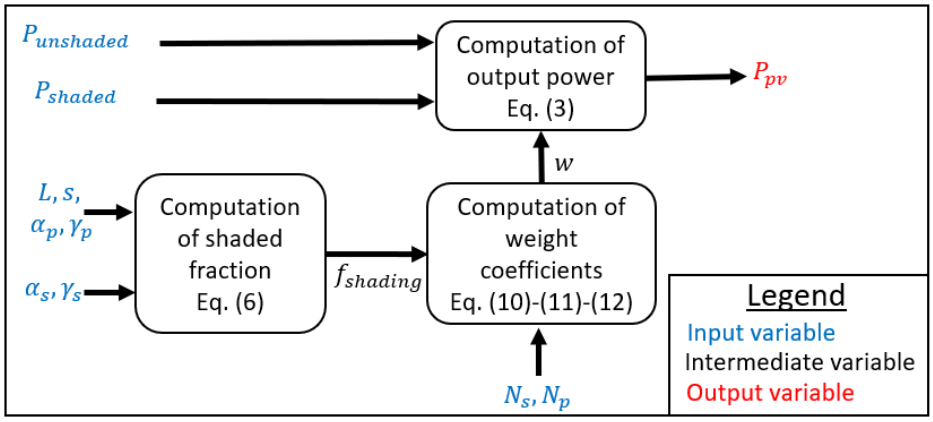

Figure 5: Illustration of the different steps of the proposed model for the effect of row-to-row shading.

3.2 Shaded fraction calculation

3.2.1 Calculation details

Calculating the shaded fraction requires knowledge on the two angles determining the sun position: the solar azimuth angle (α_s) and the sun elevation angle (γ_s). These two angles are calculated using the geographical coordinates of the PV plant and the time according to the set of equation provided by e.g. [12].

For geometric calculations, we assume a solar plant with parallel rows of infinite length on a flat ground. The shading behaviour along the module row is thus homogeneous and we can conduct the calculation in any cross section of the PV array. As illustrated in Figure 6, we chose the plane encompassing the normal to the ground and the sun direction's vector. The assumption of infinite rows implies neglecting the difference in shading at the beginning and end of the rows. It represents thus an acceptable approximation for long rows but can bring about large errors for small PV systems.

To calculate the shaded fraction, several pieces of information on the configuration of the PV plant are needed: the tilt and azimuth angles of the PV modules (γ_P,α_P), the panel length (L) and height (H) and the row spacing distance (s). These quantities are illustrated in Figure 1.

Now that all needed quantities are introduced, the shaded fraction of the module area ($f_{shading}$) can be calculated with simple geometrical considerations in the plane including normal to the ground and the sun orientation vector. This plane is represented by a red rectangle in the left picture of Figure 6, where a three-dimensional representation of the problem is provided. We consider two module rows, whose intersection with the considered plane are marked by the segments [BC] and [EF] in the right picture of Figure 6. In this two-dimensional representation, the points 0, D and A are respectively the origin, the projection of the shade of the point B on the second module row and on the ground.

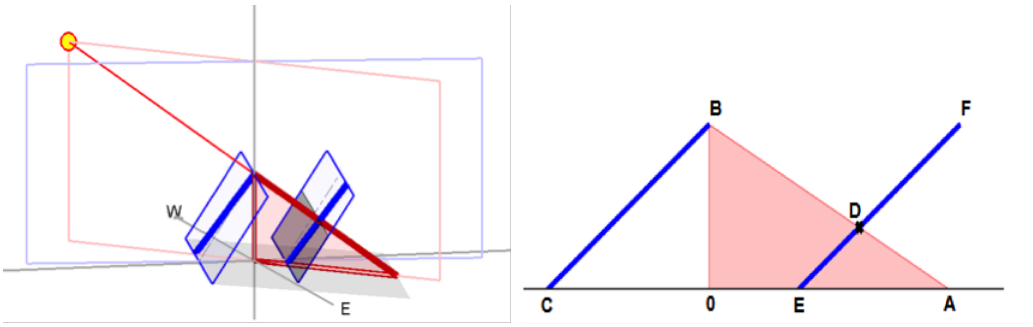

Figure 6: Illustration of the lengths used for the calculation of the shaded fraction in the space (left) and in the plane including the sun and the origin (right).

Assuming an infinite module length, the shaded fraction of the module area is equal to the ratio of the distances DE and EF, or, having BC=EF, to the ratio of the distances DE to BC ($f_{shading} = DE/BC$). To determine this ratio, we consider the two triangles (ABC) and (ADE). The lines (BC) and (EF) being parallel, according to the intercept theorem, the ratio of lengths DE/BC is equal to EA/AC, so we have:

$$f_{shading} = \frac{DE}{EF} = \frac{DE}{BC} = \frac{EA}{AC} = \frac{OA - OE}{OA + OC} \tag{4}$$

The three lengths OA, OE and OC can be easily calculated by geometrical considerations (see A) and we have:

$$\begin{aligned} OA &= Lsin(\gamma_P)/tan(\gamma_s) \\ OE &= s/cos(\alpha_s - \alpha_P - \pi) \\ OC &= Lcos(\gamma_P)/cos(\alpha_s - \alpha_P - \pi) \end{aligned} \tag{5}$$

Finally, using equations 4 and 5, the shaded fraction of the module area can be expressed as follows:

$$f_{shading} = \left[\frac{|Lsin(\gamma_P)/tan(\gamma_s)| - |s/cos(\alpha_s - \alpha_P - \pi)|}{|Lsin(\gamma_P)/tan(\gamma_s)| + |Lcos(\gamma_P)/cos(\alpha_s - \alpha_P - \pi)|} \right] \text{ if } |\gamma_s - \gamma_P| < \pi/2$$
$$0 \text{ if } [|\gamma_s - \gamma_P| \geq \pi/2 \text{ or } \gamma_s < 0] \tag{6}$$

Where:

- α_s is the sun azimuth angle [°]
- γ_S is the sun elevation angle [°]
- α_P is the module azimuth angle [°]
- γ_P is the module tilt angle [°]
- L is the panel length [m]
- s is the module row interspacing distance [m]

3.2.2 Validation of the shaded fraction calculation

The shaded fraction has been calculated with equation 6 for the two PV plants Delitzsch and Althen. The results are displayed in the two upper pictures of Figure 7, where the shaded fraction is represented by colours as a function of the sun azimuth and elevation angles. The two lower plots of the same figure show the ratio of the measured to simulated unshaded power as a function of the sun position. This ratio has been used in order to display the effect of shading without being affected by the changes of the sun position with time. In the two latter plots, the points have been sorted by decreasing diffuse fraction so that the visualization of the data focuses on situations where the effect of shading on the power is at the highest.

It can be observed that areas with shaded fraction equal to zero (grey area in the left pictures of Figure 7) correspond to regions where the ratio of measured to simulated unshaded power is higher than 0.8. In contrast, sun

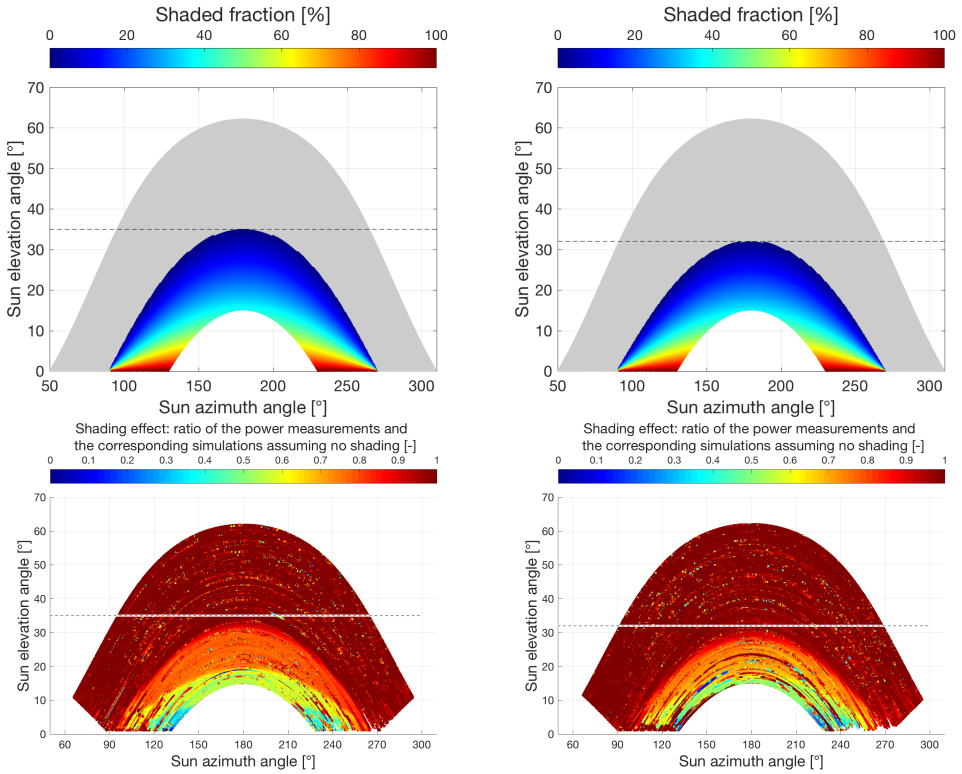

Figure 7: Comparison of the calculated shaded fraction (top plots) with the ratio of shaded to unshaded power values (bottom plots). Left column: Delitzsch. Right column: Althen.

positions with a shaded fraction greater than zero corresponds to ratio values less than 0.8. The calculated values of the shaded fraction are therefore in good agreement with the power measurements. A comparison of the two rows of plots shows that while the evolution of the shaded fraction is continuous, that of the ratio of measured to simulated unshaded power values exhibits discontinuities. This behaviour of the power values are stemming from the interconnection of the cells and will be further analyzed and discussed in the following subsections.

3.3 Comprehensive analysis of the effect of inter-row shading on the PV power generation

3.3.1 Data analysis of the power measurements

So far, we have clearly identified that the shaded fraction and the amount of direct fraction are two important predictors of the effect of inter-row shading

on the power production. In addition, we have observed that the evolution of power production with increasing shaded fraction is non-linear. The objective of this section is to further analyze the relationship between power measurements, share of direct irradiation in the POA and shading fraction as a preliminary to the development of an inter-row shading model. Indeed, we want our model to be as simple and accurate as possible, for which purpose a good understanding of the data is important.

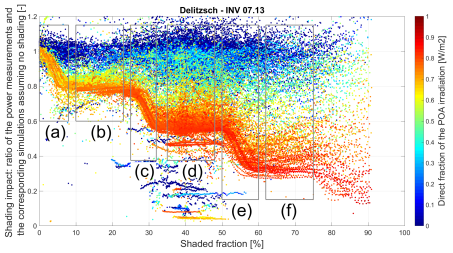

(i) Delitzch - all data

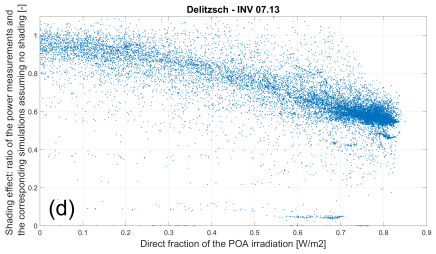

(ii) Delitzch - region (d)

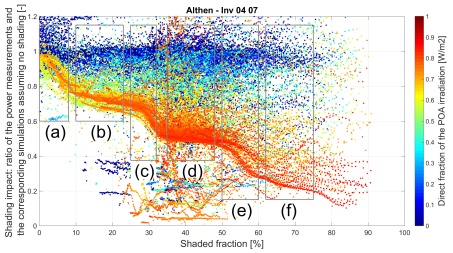

(iii) Althen - all data

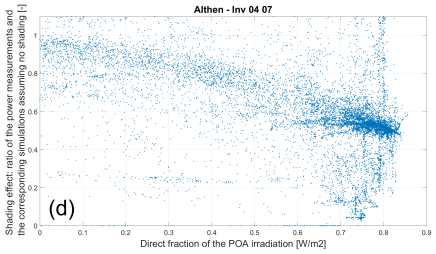

(iv) Althen - region (d)

Figure 8: Plots (i) and (iii): dependency between the ratio of measured to simulated unshaded power values and the percent of array shaded at Delitzsch and Althen. The colours of the scatter points represent the share of direct irradiation in the global POA irradiation and 5 regions are marked from (a) to (f) for the discussion of the plots. Plots (ii) and (iv): evolution of the ratio of measured to simulated unshaded power values with the direct fraction for shaded fraction values comprised between 35 and 45% in Delitzsch and Althen (data corresponding to the region (d) in plots (i) and (iii)

Power measurements are first displayed as a function of the shading fraction and the direct fraction of the POA in the different plots of Figure 8. Upper plots corresponds to Delitzsch and lower ones to Althen. In order to directly observe the shading effect and get rid of the effect of the change of the sun position on the power, the ratio of the measurements and the shading free power simulation are considered instead of the power measurements. This ratio is referred to as "shading impact" in the following of the text. In the first column of plots, this ratio is displayed as a function of the shaded

fraction whereby the colours of the scatter points represent the fraction of direct irradiation in the POA irradiation. To ease the analysis of this first two figures, six regions corresponding to different values of shaded fraction are marked from (a) to (f). In the second column of plots, the evolution of the ratio of measurements to shading free simulation (shading impact) is displayed as a function of the share of direct irradiation in the POA irradiation for the region (d) introduced above (shaded fraction comprised between 35 and 45%).

When the direct POA irradiation is very low (blue points in the two plots of the left column), the dependency between the shading impact and the shaded fraction is very small: the values of the shaded impact are distributed around unity for all values of the shaded fraction. As the share of direct fraction increases, a dependency between the two quantities appears until exhibiting a step-wise behaviour for great values of the direct fraction (red points in the left column in Figure 8). As illustrated in the two plots on the right column, the transition between these two extreme situations is linear for the region (d). The visual inspection of the data shows that the same observation holds for other values of the shaded fraction. Based on this observation, it appears reasonable to consider that the effect of the shading on the power increases proportionally with the direct fraction of the POA irradiation, which validates our modelling approach expressed in Eq. 3.

We now focus on the dependency between power reduction and shaded fraction for scatter points strongly affected by shading (red points). It can be observed in the two plots that the red points follow a pattern that repeats regularly along the diagonal. The first pattern consists of the regions a) and b) for shaded fraction between 0 and 0.25, the second of regions c) and d) for shaded fraction between 0.25 and 0.5 and finally the third of the regions e) and f) for shaded fraction between 0.5 and 0.75. As suggested by their vertical and horizontal extensions (both equal to ca. 0.25), these patterns corresponds to the individual effect of each of the four rows of panels on the production of the total array. The structures formed by the red points suggest that the contribution of the four row connected in parallel can be considered independent as a first approximation: the power production of rows connected in parallel could therefore be calculated independently and summed up to assess the inverter power production.

It can be observed that the power is very sensitive to shading in the regions (a), (c) and (e) while this sensitivity is very small in the regions (b), (d) and (f). This behavior is well known: the reverse current of the shaded cell limits the current of the whole string. As a result, all cells - even unshaded ones - operate at the same operating point as shaded cells. Once a cell is fully shaded, incremental shading of further cells has no more effect

Technology	c-Si
STC power	210 W
photocurrent (@STC)	$I_L = 5.658A$
dark current	I0 = 4.629E-11 A
shunt resistance	$R_{sh} = 269.68$
series resistance	$R_s = 0.386$
ideality factor	n=1.0134
number of cells in series	$N_s = 72$
module temperature	$T_{mod} = 25°C$
global horizontal irradiance	GHI= 1000 W/m^2
diffuse fraction	$K_d = 15\%$

Table 2: Characteristics of the PV module used for the IV calculations

on the string power which explains the shape of the regions (b), (d) and (f). This interpretation is confirmed by the width of regions (a), (c) and (e) that are all close to 100/4/6=4.16% (100% of the module area divided by 4 module rows and by 6 rows of cells per module).

We can note a difference between the two plants in the evolution of the shading impact with the shaded fraction for the regions (b), (d) and (f): while the shaded fraction is constant in Delitzsch, it decreases steadily in Althen. This effect may result from module mismatch effect and/or activation of the bypass diodes but the actual causes of this different behavior couldn't be identified with the set of information available for the two plants.

3.3.2 Simulation-based analysis of the role of the cell interconnection and bypass diodes on the shading losses

To validate the interpretations made in the previous section and deepen the understanding of the role of array configuration on the shading losses, numerical experiments have been conducted whose main results are summarized here. The PV-lib library [28] has been used to generate the IV curve of a PV cell including its reverse current. The characteristics of the standard cell included in the library have been used (see Table 2).

In order to consider the effect of shading, the solar radiation effectively contributing to the light current generated by a partially shaded cell is evaluated as a function of the shading fraction as follows:

$$G_{eff} = G \times K_d + G \times (1 - K_d) \times (1 - f_{shading,cell}); \quad (7)$$

With :

- G_{eff} : effective irradiance on the module
- G : irradiance in the module without shading effect
- K_d : diffuse fraction
- $f_{shading,cell}$: shaded fraction of the cell

The value of $f_{shading,cell}$ has been evaluated for each cell using the geometry of the considered array and the shaded fraction $f_{shading}$, which refers to the entire array.

In a first step, we evaluate the evolution of the power generated by a single cell as the shaded fraction increases. This first case is trivial but it is aimed at explaining our approach. The results are given in Figure 9a. The experimental setup is illustrated in the left image of this figure and, in the middle plot, the evolution of the IV curve with the shaded fraction is displayed using a colour system representing the level of shading. The maximum power points are also represented by black circles in this figure. The evolution of the power with the shaded fraction is finally represented on the right picture of Figure 9a. As expected in this first case, it can be observed that the power is decreasing linearly with the shaded fraction.

In a second step, the effect of shading on an horizontal module without bypass diode is evaluated. The results are shown in Figure 9b. Since no bypass diode is used, for a given voltage, the maximal current is set by the most shaded cell, which therefore limits the whole module. Once a cell is fully shaded the loss is at its highest and a further increase of the shading has no further impact on the module power production.

In a third step, we consider a module with three bypass diodes, which prevent shaded cells to operate as loads. The effect of the three bypass diodes on the module IV curve can be clearly observed in the middle plot of Figure 9c. In this case, the shadow brings about two local maximum power points in the IV curve. With increasing shaded fraction, the maximum power alternates between the two maxima: a local maximum where the power decreases rapidly with the shaded fraction and a local maximum where the power is independent on the shaded fraction.

In the fourth and fifth experiments, the effect of partial shading on arrays with and without bypass diodes are investigated respectively. For this purpose, four similar modules connected in parallel are considered. A string with a larger number of modules would have been more realistic but a single module string was chosen to allow a better visualization of the effect of the bypass diodes on the IV curves. The results are displayed in the Figures 10a and 10b. It is interesting to note that while the effect of the bypass diodes on

the IV curve is clearly observable (middle plot of Figure 10a), the influence of bypass diodes on the relationship between power production and shaded fraction is much less marked, especially for shaded fraction under 50%.

In order to get a better insight on the effect of bypass diodes on partially shaded module arrays, we have superposed in Figure 11 isolines of constant power to the curves of Figure 10a. With this representation, the logic behind the activation of the bypass diodes becomes clear. For low values of the shaded fraction, the gain in current resulting from the activation of the bypass diode is not sufficient to balance out the voltage decrease. In this case, among the two local power maxima resulting from the effect of the bypass diode, that corresponding to the global maximum has the higher voltage: it is thus the operating point where the bypass diode is not activated. When the shaded fraction increases, the two local maxima become very close so that activation of the bypass diodes can be observed. For values shaded fraction greater than 0.5, the effect of the bypass diode becomes indeed clearly visible: an intermediary step can be seen for shaded fraction values between 0.55 and 0.6 and between 0.75 a 0.85. It should however be noted that the activation of the bypass diodes is dependent on the shape of the IV curve of individual cells and therefore on their electrical characteristics. Further analysis would be interesting to get a better insight on this issue but we decided not to conduct further numerical experiments.

Finally, the effect of shading for a portrait oriented PV module is displayed in Figure 10c. Here again, the total power production is limited by the current of the most shaded cell which is more penalizing in this configuration.

In this section, we considered strings made of a single PV module to facilitate the visualization of the results. It can however be noted that if different modules connected in series are facing identical shading, their respective IV curve will be identical and the behaviour of the string will be the same as that of a single module. The effect of shading will however be smoothed out by difference in shading fraction or electrical characteristics within the string. This may be a possible explanation for the decrease observed for the Althen plant in Figure 8.

3.4 Modelling approach

Our model is a linear combination of the two power values $P_{unshaded}$ and P_{shaded}, that corresponds respectively to the power production without shading and with a complete shading. The respective influences of the two power values on the simulated output power are modulated by a weighting coefficient w:

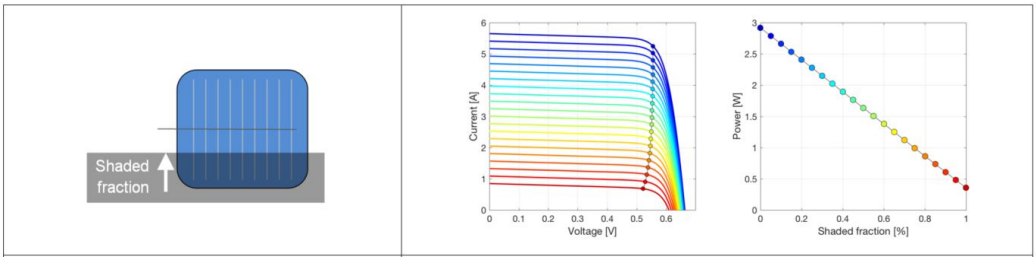

(a) Effect of a partial shading on the power output of a PV cell

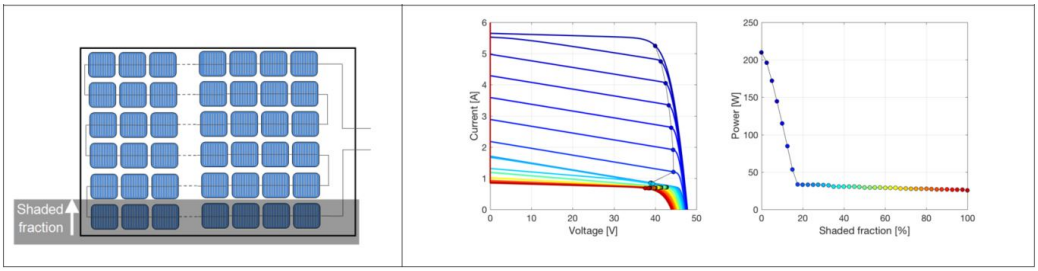

(b) Effect of a partial shading on the power output of a landscape oriented PV module without bypass diodes

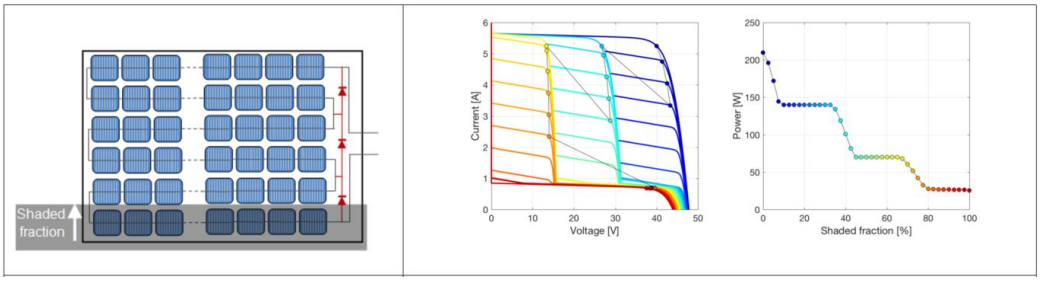

(c) Effect of a partial shading on the power output of a landscape oriented PV module with three bypass diodes

Figure 9: Result of numerical experiments on different interconnection layouts (Part 1/2)

$$P_{pv} = w \times P_{unshaded} + (1 - w) \times P_{shaded} \tag{8}$$

The weighting coefficient w is the sum of two components: a first component $w_{FullyUnshaded}$ accounting for all strings that are not affected by the shading and a second component $w_{PartiallyShaded}$ accounting for the string that is partially shaded:

$$w = w_{FullyUnhaded} + w_{PartiallyShaded} \tag{9}$$

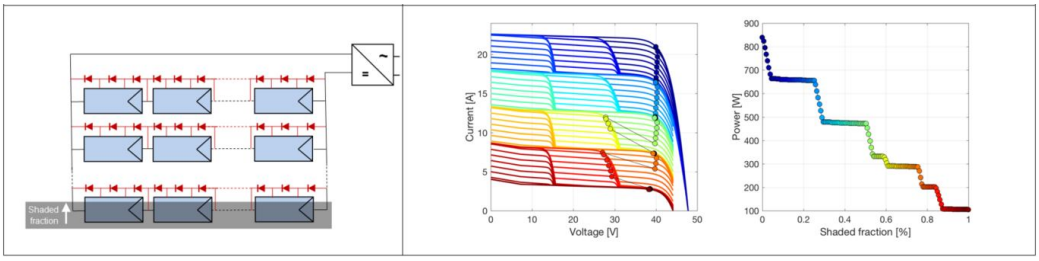

(a) Effect of a partial shading on the power output of four parallel strings with landscape panel with three by pass diodes per module

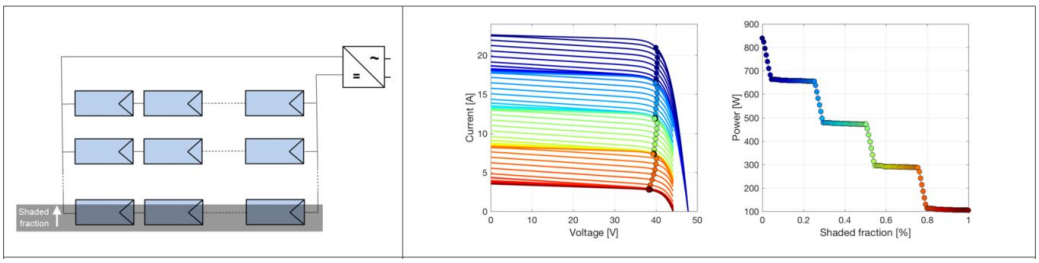

(b) Effect of a partial shading on the power output of four parallel strings without by pass diode

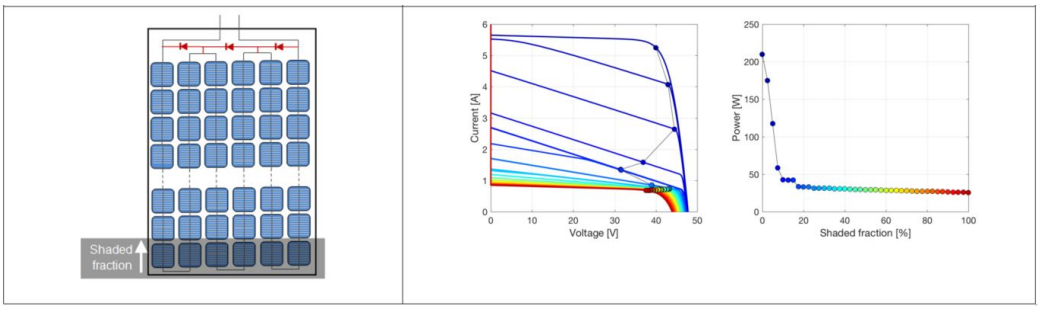

(c) Effect of a partial shading on the power output of portrait oriented module (with or without bypass diode)

Figure 10: Result of numerical experiments on different interconnection layouts (Part 2/2)

Illustration of a unshaded, partially and fully shaded strings are presented in Figure 14 in B.

The first term, $w_{FullyUnshaded}$, can be interpreted as the share of parallel strings of the system that are not affected by the shading. It can be expressed as a function of the number of parallel string N_p and the shaded fraction $f_{shading}$ as follows:

$$w_{FullyUnshaded} = 1 - \lceil f_{shading} \times N_p \rceil / N_p; \tag{10}$$

In the above expression, the operator $\lceil \quad \rceil$ represents the ceiling function

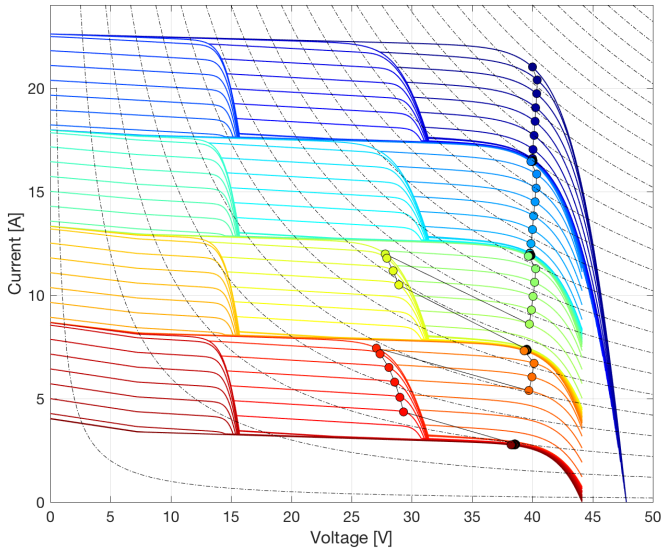

Figure 11: Superposition of isolines of constant power to the plot illustrating the effect of shading on the IV curve of an array equipped with bypass diodes (figure 9c).

that takes as input a real number x and gives as output the least integer greater than or equal to x. The evolution of $w_{FullyUnshaded}$ with the shaded fraction is represented by a blue area in Figure 12.

The second term, $w_{PartiallyShaded}$, can be interpreted as the relative contribution of the direct irradiation to the power production of the partially shaded string. To calculate this second component of the weight, we need to consider the number N_s of cells connected in series along the vertical. For example, N_s is equal to 6 a module with 6 x 12 cells oriented in landscape. If the same model has a portrait orientation, then N_s is equal to 12. Using the newly introduced parameter, N_s, as well as the shaded fraction $f_{shading}$ and the first weight term $w_{FullyUnShaded}$, the second component of the weighting coefficient $w_{PartiallyShaded}$ can be expressed as follows:

$$w_{PartiallyShaded} = max(0, [(1 - f_{shading}) - w_{FullyUnshaded}] \times N_s - \frac{N_s - 1}{N_p}) \quad (11)$$

The evolution of $w_{PartiallyShaded}$ with the shaded fraction is represented by a red area in Figure 12.

The calculation of the weight for types of configurations is given in B, which is intended are clarifying our modelling approach through examples.

For each given example, the parameters N_s and N_s are given and the evolution of the two components of the weight as a function of the shaded fraction are provided.

The modelling approach described in this section suits well the behaviour observed for the Delitzsch plant but the slow decrease for the power production with shaded fraction observed for Althen plant is not reflected by our model. This is due to the fact that the effect of the bypass diodes is not taken into consideration since we judge that the added modelling complexity and required input parameter is not justified by the added modelling accuracy. As a result, our model is, in its current form, a lower bound of the power production that can occur when bypass diodes are activated. Nevertheless, based on the data analysis, we consider that it describes the main effect of shading on the power output of a PV plant.

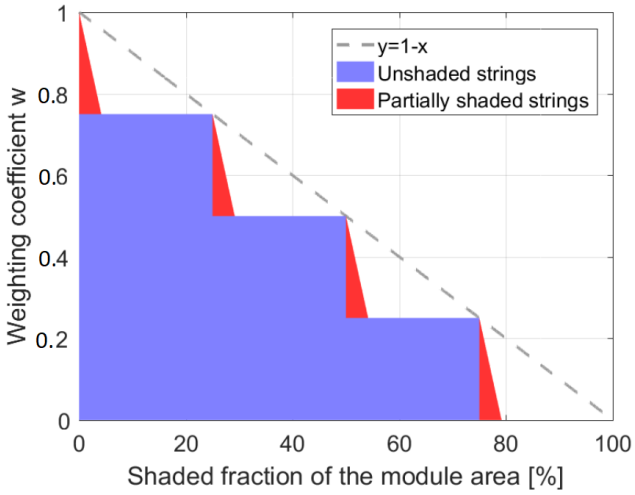

Figure 12: Illustration of the evolution of the weighting factor w with the shaded fraction of the module area $f_{shading}$, in the example of four parallel strings with 6x12 cells panel in landscape (same example as 19 B. The violet part corresponds to the contribution of the unshaded strings, the red part corresponds to the contribution of the partially shaded one.

4 Evaluation of the model performances

The targeted application of our model is instantaneous calculation, where advanced calculation methods involving combination of individual IV curves is not feasible. In such cases, two options are usually considered: the use

of a simple physical model where the impact of shading is neglected or the use of statistical models. The consideration of statistical model being out of the scope of the present study, we will use the calculation based on a simple physical model as a reference case in this validation.

As a result, we will compare the output of the model described in the previous section with the time series of the simulated power values assuming a shading free environment ($P_{unshaded}$) that has already been introduced. The two simulated time series are compared against the power measurements for the two plants in Figure 13. The simulated values are displayed on the ordinate and the measured values on the abscissa. The colours of the scatter points represent the local density of scatter points. Only points corresponding to a sun elevation less than 35° have been displayed in this figures in order to better visualize the shading effect on the scatter plots.

It can be observed in the four plots of Figure 13 that the dispersion of the scatter points is relatively high. This noise results from the mismatch between the used satellite-derived irradiation and the actual irradiation received by the PV modules but also from the error of the decomposition and transposition models. A systematic bias can be observed for the Althen plant, which has already been observed in Figure 3 and discussed in section 2.2. Some abnormal values resulting from operation failures can also be observed for the Althen PV plant in this figure.

Regions corresponding to an overestimation of the power generation by simulated power without consideration of inter-row shading can be observed in the left plots of Figure 3 (e.g. measured power of 0.3 for a simulated power of 0.5 kW/kW_p). Such overestimation are due to the effect of inter-row shading and, as shown by a comparison of the two pairs of plots, they are corrected by the use of our model.

The bias, MAE, RMSE and correlation coefficient have been evaluated for all simulations. The results are given in Table 3. The different error metrics have been evaluated for two subsets of the data: firstly, over the complete time period (without night values) and, secondly, only for time steps when inter-row shading occurs ($f_{shading} > 0$).

The improvement obtained by considering inter-row shading is the higher for Delitzsch with a relative decrease of the RMSE (MAE) of 32% (31%) and 12% (8%) for the times affected by inter-row shading ($f_{shading} > 0$) and the complete time period respectively. Though smaller, the improvement resulting from the consideration of inter-row shading is also noticeable for the Althen PV plant: the relative decrease of the RMSE (MAE) is equal to 18% (10%) and 7% (4%) for the limited and complete time periods respectively. The lower performances obtained for the Althen plant can be on the one hand explained by the different characteristics observed in Figure 8 and on the

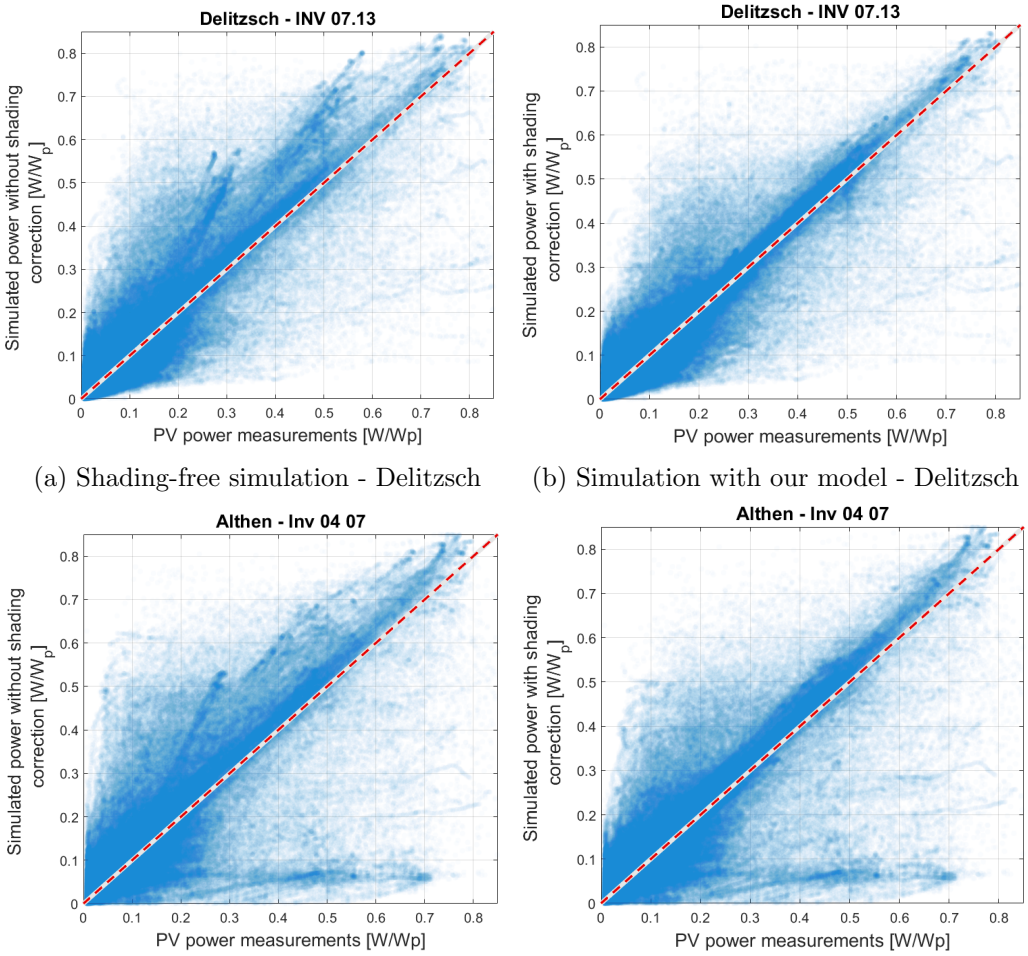

(a) Shading-free simulation - Delitzsch (b) Simulation with our model - Delitzsch

(c) Shading-free simulation - Althen (d) Simulation with our model - Althen

Figure 13: Comparison of the simulated power values (ordinate) against the corresponding measurements (abscissa) with and without consideration of the inter-row shading (left and right plots respectively) and for the Delitzsch and Althen PV plants (upper and lower plots respectively).

other hand by the issues observed in the power measurements (measurement error or line outage).

5 Conclusion

In this work, an approach for calculating the effect of inter-row shading on the PV power production has been developed with the objective to have the simplest model and the minimal number of input parameters while preserving

		Delitzsch PV plant		Althen PV plant	
		Shading-free simulation	Proposed model	Shading-free simulation	Proposed model
$\gamma_s > 0$ $f_{shading} > 0$	bias	0.0356 W/W$_p$	0.0098 W/W$_p$	0.0048 W/W$_p$	-0.0184 W/W$_p$
	MAE	0.0551 W/W$_p$	0.0370 W/W$_p$	0.0832 W/W$_p$	0.0684 W/W$_p$
	RMSE	0.0886 W/W$_p$	0.0612 W/W$_p$	0.1395 W/W$_p$	0.1260 W/W$_p$
	corr	0.8911	0.9063	0.6240	0.6369
$\gamma_s > 0$ $f_{shading} \geq 0$	bias	0.0212 W/W$_p$	0.0096 W/W$_p$	0.0161 W/W$_p$	0.0072 W/W$_p$
	MAE	0.0669 W/W$_p$	0.0588 W/W$_p$	0.0803 W/W$_p$	0.0747 W/W$_p$
	RMSE	0.1080 W/W$_p$	0.0992 W/W$_p$	0.1298 W/W$_p$	0.1244 W/W$_p$
	corr	0.8947	0.9059	0.8546	0.8625

Table 3: Comparison of the simulation error with and without consideration of effect of the inter row shading on the PV power production

the modelling accuracy. This objective has been pursued by motivating the modelling approach by a data analysis of power measurements of two large PV plants. The present work thus includes both a model development and a comprehensive data analysis.

We found a modelling approach consisting in the linear combination of the power values corresponding to a fully shaded and fully shaded environment. The weighting coefficient is a simple parametric expression depending on two configuration parameters and the shaded fraction of the modules. The configuration parameters summarize the interconnection of the cells within the array: the number of strings in parallel and the number of cells in series along the vertical of the modules. These two parameters should be relatively easy to assess and, in case they are not known, they can be inferred using the data analysis procedure described in this paper. A parametric expression based on geometric calculation is proposed for the shading fraction. We also propose a method for calculating the power values corresponding to a fully shaded and an unshaded environment, though it is possible to use any other method instead.

The relative improvement of the simulation accuracy (RMSE) obtained by the implementation of the proposed model ranges between 18 and 32% for time steps affected by inter-row shading ($f_{shading} > 0$) and between 7 and 12% for the complete year. A noticeable effect can also be observed in the scatter plot of simulated against measured power, where the consideration of inter-row shading mitigates the occurrence of numerous values with an overestimation of the power generation.

In the proposed approach, we used satellite derived global horizontal ir-

radiation (GHI) to evaluate the direct and diffuse fraction of the POA irradiation. The use of external data was necessary because only POA irradiation is measured and no GHI measurements is available. The uncertainty of the satellite data brings about noise in our model which is unfortunate since this noise is stemming from the satellite data and not from our model.

The model has been validated using two relatively similar PV plant configurations. It would be interesting to validate and eventually extend the proposed model for further plant architecture (e.g. total cross tie, bridge link architectures). An extension of the calculation of the diffuse fraction for a tilted ground could also be considered in the future.

Acknowledgements

The authors would like to thankfully acknowledge Enerparc AG for providing the plant measurements and the friendly cooperation. We would like to also thank Transvalor for giving us access to satellite-derived irradiation data.

References

References

[1] WR Baron and PF Virobik. Solar array shading and a method of reducing the associated power loss. *NASA technical report server document 19640022825 http://ntrs. nasa. gov/index. jsp*, 1964.

[2] F. Belhachat and C. Larbes. Modeling, analysis and comparison of solar photovoltaic array configurations under partial shading conditions. *Solar Energy*, 120:399 – 418, 2015.

[3] H. G. Beyer, J. Bethke, A. Drews, D. Heinemann, E. Lorenz, G. Heilscher, and S. Bofinger. Identification of a general model for the mpp performance of pv-modules for the application in a procedure for the performance check of grid connected systems. In *Proc. 19th European Photovoltaic Solar Energy Conference and Exhibition, Paris, France, 2004*, Paris, France, 2004.

[4] JW Bishop. Computer simulation of the effects of electrical mismatches in photovoltaic cell interconnection circuits. *Solar cells*, 25(1):73–89, 1988.

[5] Matthew Culligan and Jonathan Botkin. Impact of tilt angle on system economics for area constrained rooftops. *SunPower White Paper*, 2007.

[6] Chris Deline, Aron Dobos, Steven Janzou, Jenya Meydbray, and Matt Donovan. A simplified model of uniform shading in large photovoltaic arrays. *Solar Energy*, 96:274 – 282, 2013.

[7] DGS. *Planning and installing photovoltaic systems: a guide for installers, architects and engineers*. Routledge, 2013.

[8] M. Gostein, B. Stueve, K. Passow, and A. Panchula. Evaluating a model to estimate ghi, dni, amp;amp; dhi from poa irradiance. In *2016 IEEE 43rd Photovoltaic Specialists Conference (PVSC)*, pages 0943–0946, June 2016.

[9] Benoît Gschwind, Lionel Ménard, Michel Albuisson, and Lucien Wald. Converting a successful research project into a sustainable service: The case of the soda web service. *Environmental Modelling Software*, 21(11):1555 – 1561, 2006. Environmental Informatics.

[10] F. Iannone, G. Noviello, and A. Sarno. Monte carlo techniques to analyse the electrical mismatch losses in large-scale photovoltaic generators. *Solar Energy*, 62(2):85 – 92, 1998.

[11] INSEL, 2018.

[12] Muhammad Iqbal, editor. *An Introduction to Solar Radiation*. Academic Press, 1983.

[13] DL King, JK Dudley, and WE Boyson. Pvsim {copyright}: A simulation program for photovoltaic cells, modules, and arrays. Technical report, Sandia National Labs., Albuquerque, NM (United States), 1996.

[14] W Luft. Partial shading of silicon solar cell converter panels. In *AIEE Conf.*, 1961.

[15] Bill Marion. A model for deriving the direct normal and diffuse horizontal irradiance from the global tilted irradiance. *Solar Energy*, 122:1037 – 1046, 2015.

[16] F. Martínez-Moreno, J. Muñoz, and E. Lorenzo. Experimental model to estimate shading losses on pv arrays. *Solar Energy Materials and Solar Cells*, 94(12):2298 – 2303, 2010.

[17] R. Perez, R. Seals, and J. Michalsky. All-weather model for sky luminance distribution—preliminary configuration and validation. *Solar Energy*, 50(3):235 – 245, 1993.

[18] Giovanni Petrone, Giovanni Spagnuolo, and Massimo Vitelli. Analytical model of mismatched photovoltaic fields by means of lambert w-function. *Solar energy materials and solar cells*, 91(18):1652–1657, 2007.

[19] PV*SOL, 2018.

[20] PVsyst, 2018.

[21] Volker Quaschning and Rolf Hanitsch. Numerical simulation of current-voltage characteristics of photovoltaic systems with shaded solar cells. *Solar Energy*, 56(6):513 – 520, 1996.

[22] Hans S Rauschenbach. Electrical output of shadowed solar arrays. *IEEE Transactions on Electron Devices*, 18(8):483–490, 1971.

[23] Jan Remund, Lucien Wald, Mireille Lefèvre, Thierry Ranchin, and John Page. Worldwide linke turbidity information. In *ISES Solar World Congress 2003*, volume 400, pages 13–p. International Solar Energy Society (ISES), 2003.

[24] C Rigollier, M Lefèvre, and L Wald. The method heliosat-2 for deriving shortwave solar radiation from satellite images. *Solar Energy*, 77(2):159 – 169, 2004.

[25] Fawzan Salem and Mohamed A. Awadallah. Detection and assessment of partial shading in photovoltaic arrays. *Journal of Electrical Systems and Information Technology*, 3(1):23 – 32, 2016.

[26] H. Schmidt and D.U. Sauer. Dc-ac converter efficiencies. corresponding to practice modelling and estimation. *Sonnenenergie, München*, 21(52):43–47, 1996.

[27] Arvid Skartveit, Jan Asle Olseth, and Marit Elisabet Tuft. An hourly diffuse fraction model with correction for variability and surface albedo. *Solar Energy*, 63(3):173 – 183, 1998.

[28] J. S. Stein. The photovoltaic performance modeling collaborative (pvpmc). In *2012 38th IEEE Photovoltaic Specialists Conference*, pages 003048–003052, June 2012.

[29] N. Thakkar, D. Cormode, V. P. A. Lonij, S. Pulver, and A. D. Cronin. A simple non-linear model for the effect of partial shade on pv systems. In *2010 35th IEEE Photovoltaic Specialists Conference*, pages 002321–002326, June 2010.

A Determination of the shaded fraction

Step 1 : Calculation in the plane including the origin and the normal to the module plane (light blue).

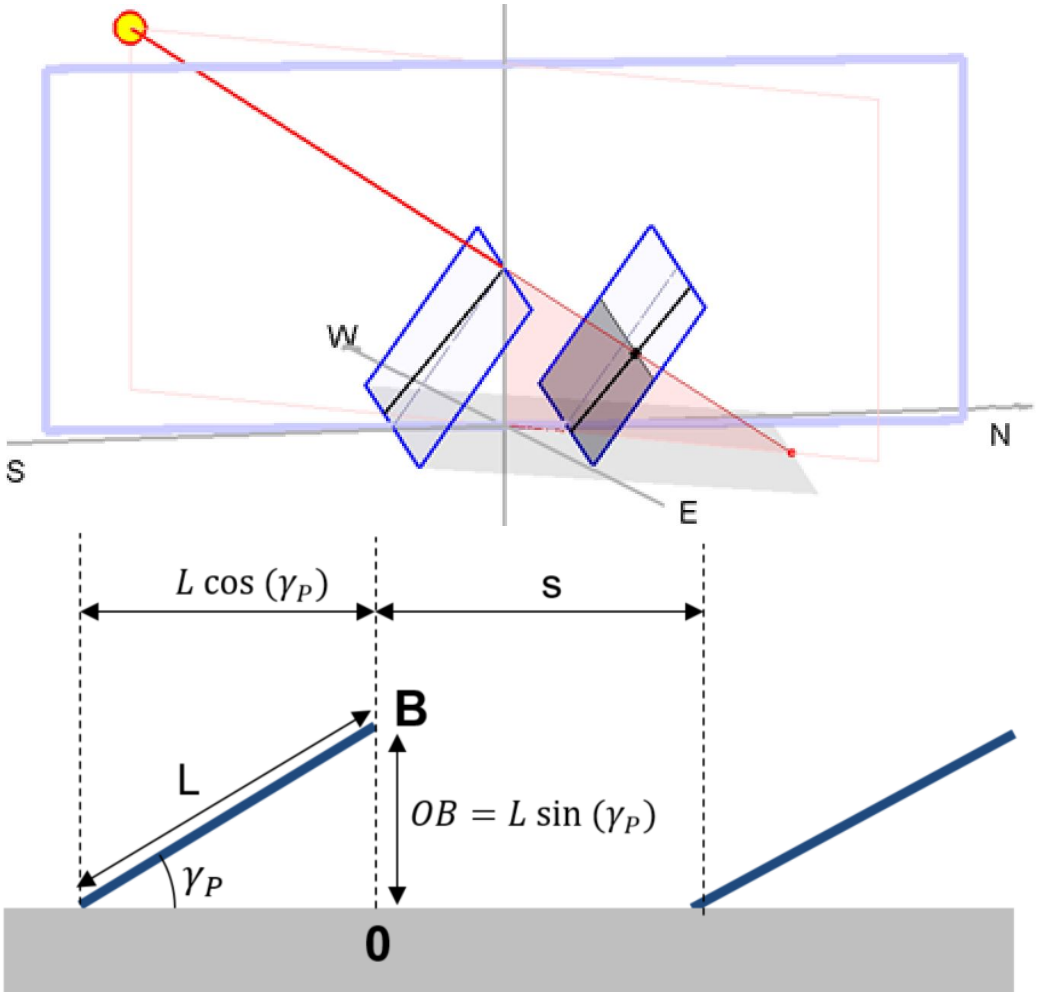

Step 2: Calculation in the horizontal plane (dark grey).

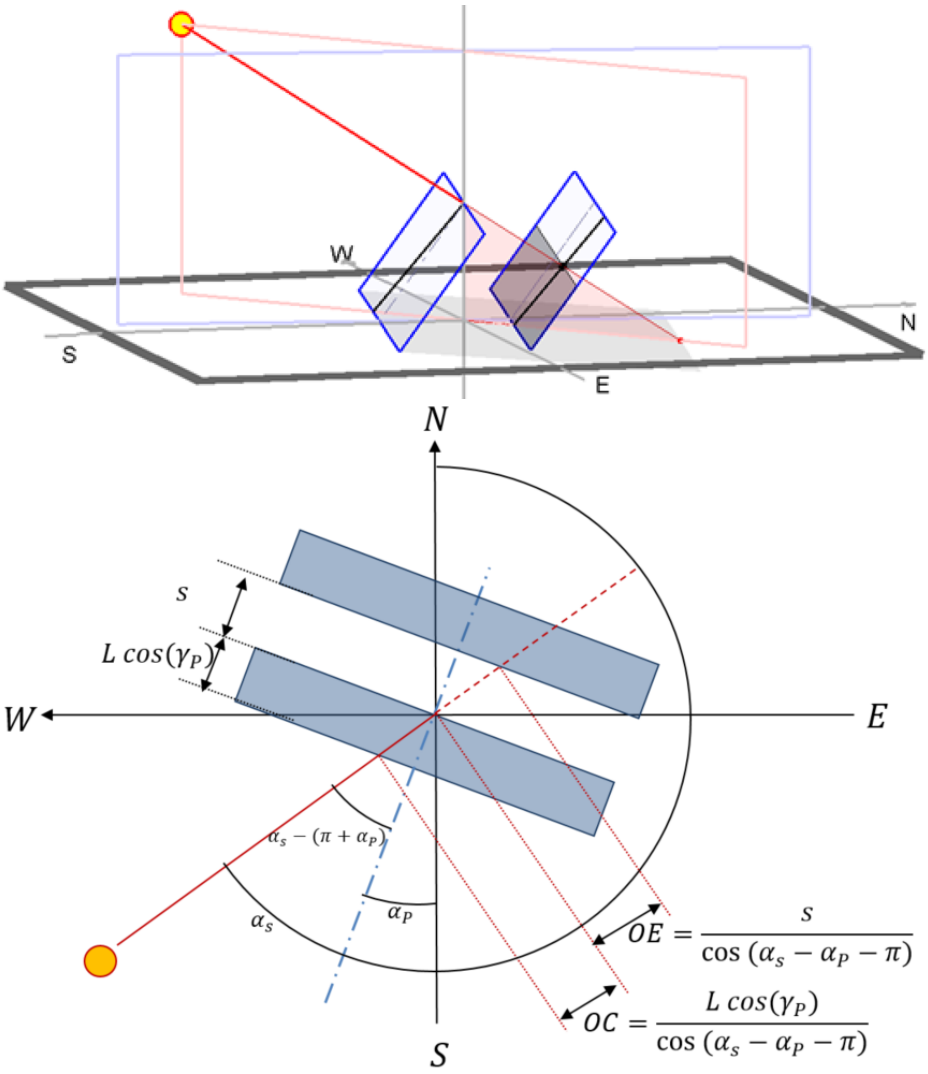

Step 3: Calculation in the plane including the sun and the vertical at the origin (light red).

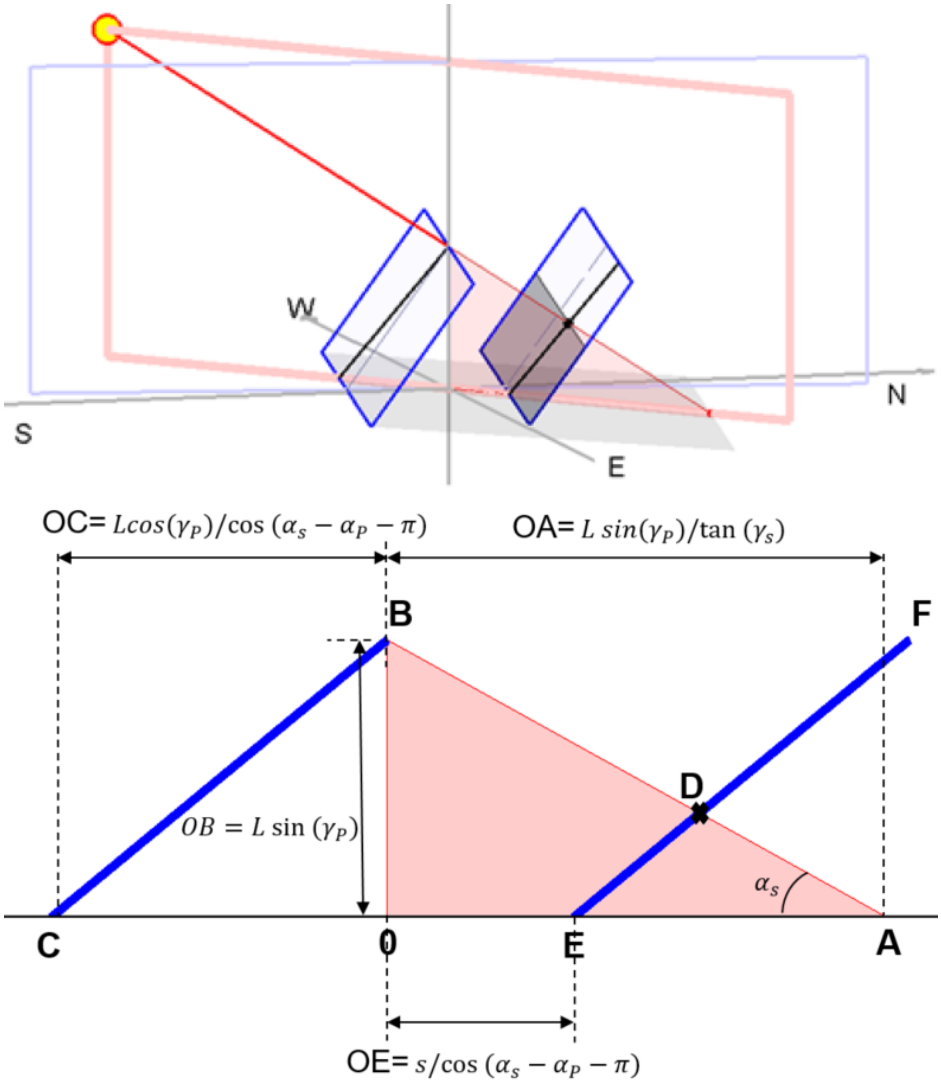

B Example of N_s and N_p, $w_{FullyShaded}$ and $w_{PartiallyShaded}$ computation

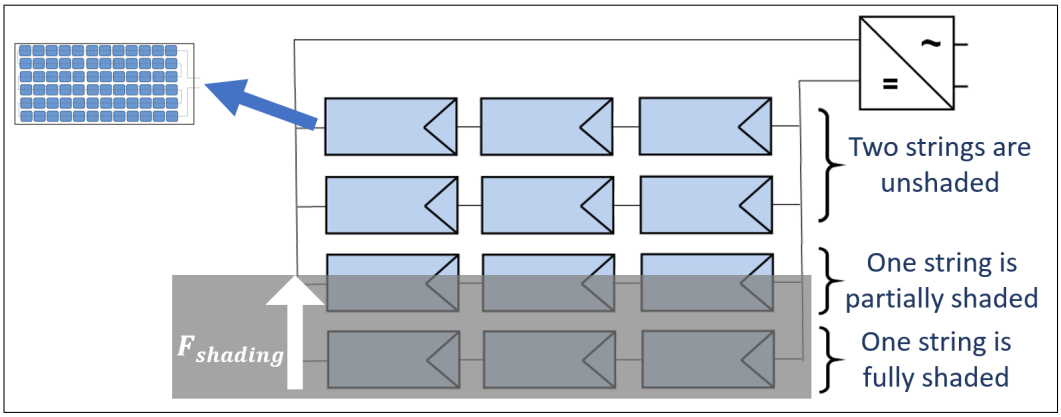

Figure 14: Illustration of an unshaded, partially and fully shaded string

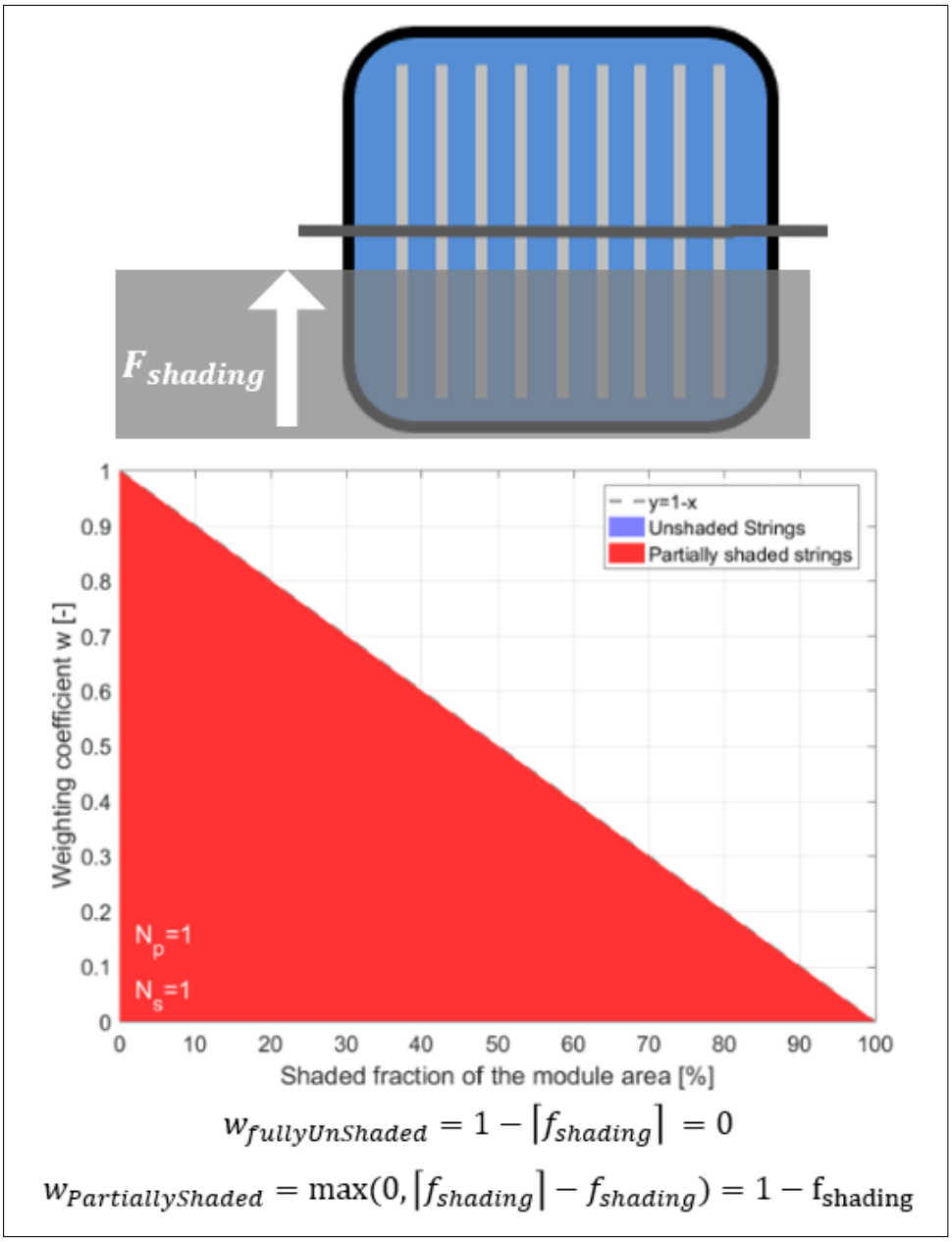

Figure 15: Example of N_s and N_p, $w_{FullyShaded}$ and $w_{PartiallyShaded}$ computation for a single cell

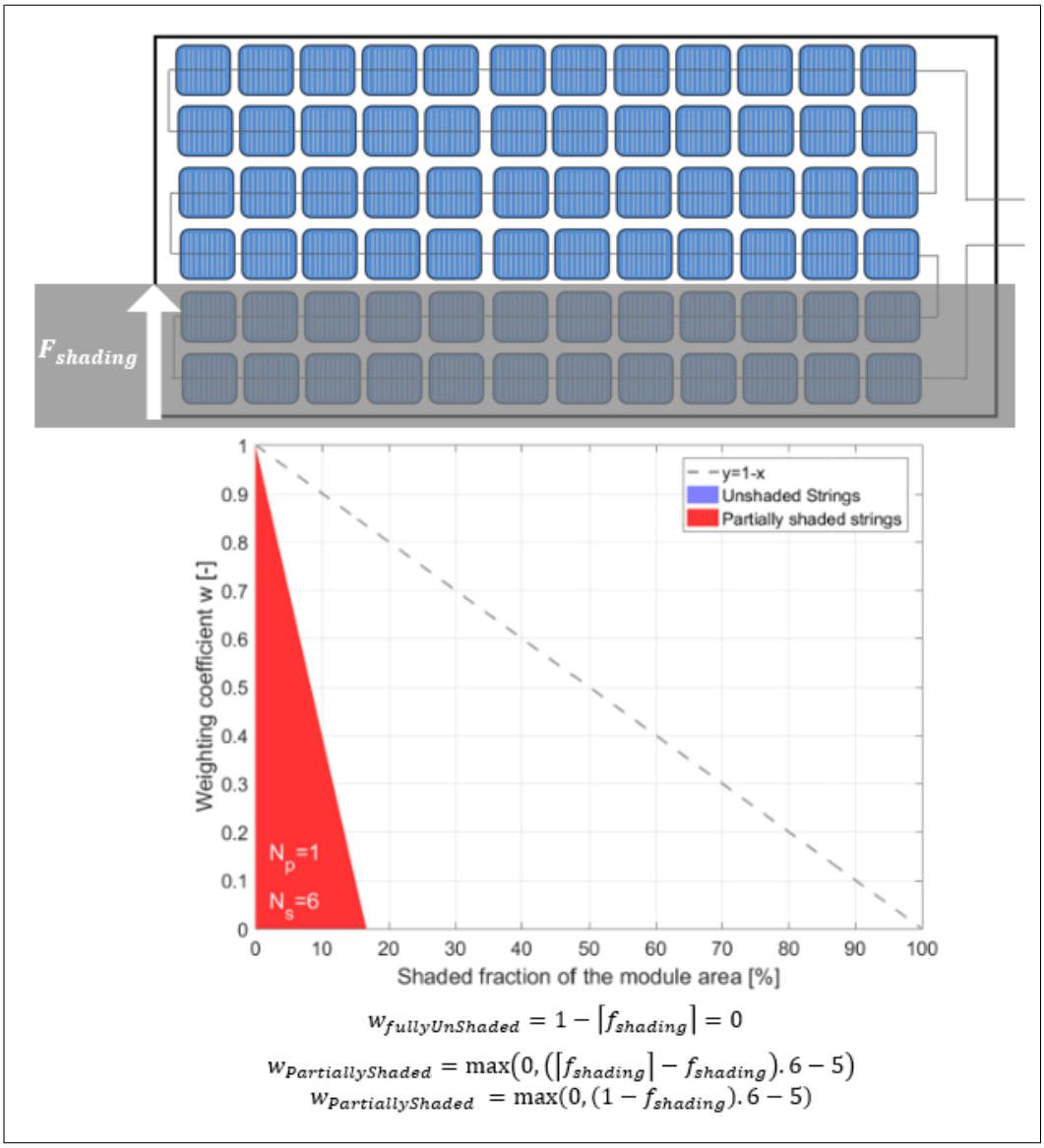

Figure 16: Example of N_s and N_p, $w_{FullyShaded}$ and $w_{PartiallyShaded}$ computation for a 6x12-cells panel in landscape orientation

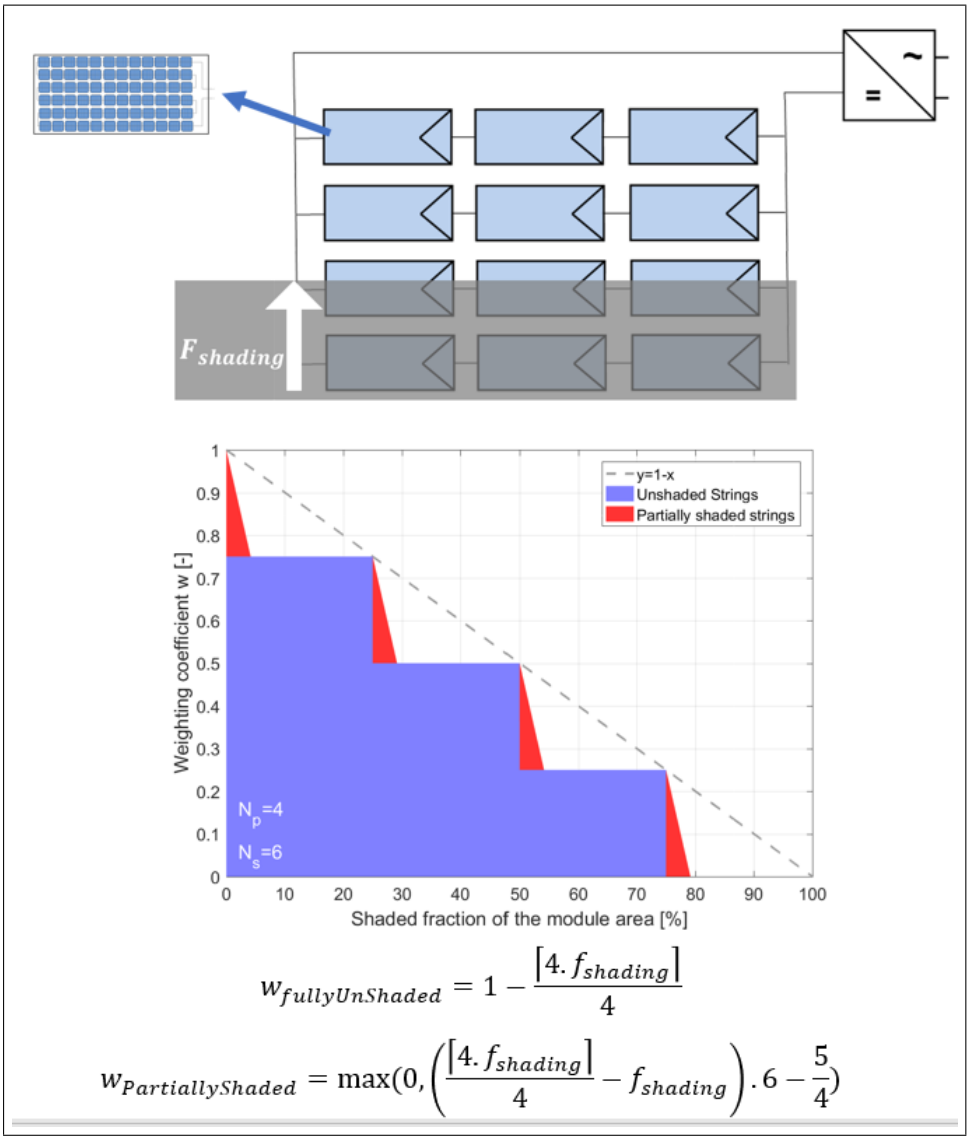

$$w_{fullyUnShaded} = 1 - \frac{\lceil 4.f_{shading} \rceil}{4}$$

$$w_{PartiallyShaded} = \max(0, \left(\frac{\lceil 4.f_{shading} \rceil}{4} - f_{shading} \right).6 - \frac{5}{4})$$

Figure 17: Example of N_s and N_p, $w_{FullyShaded}$ and $w_{PartiallyShaded}$ computation for a row of 6x12-cells panels in landscape orientation. The panel connection are 3 in series and 4 in parallel.

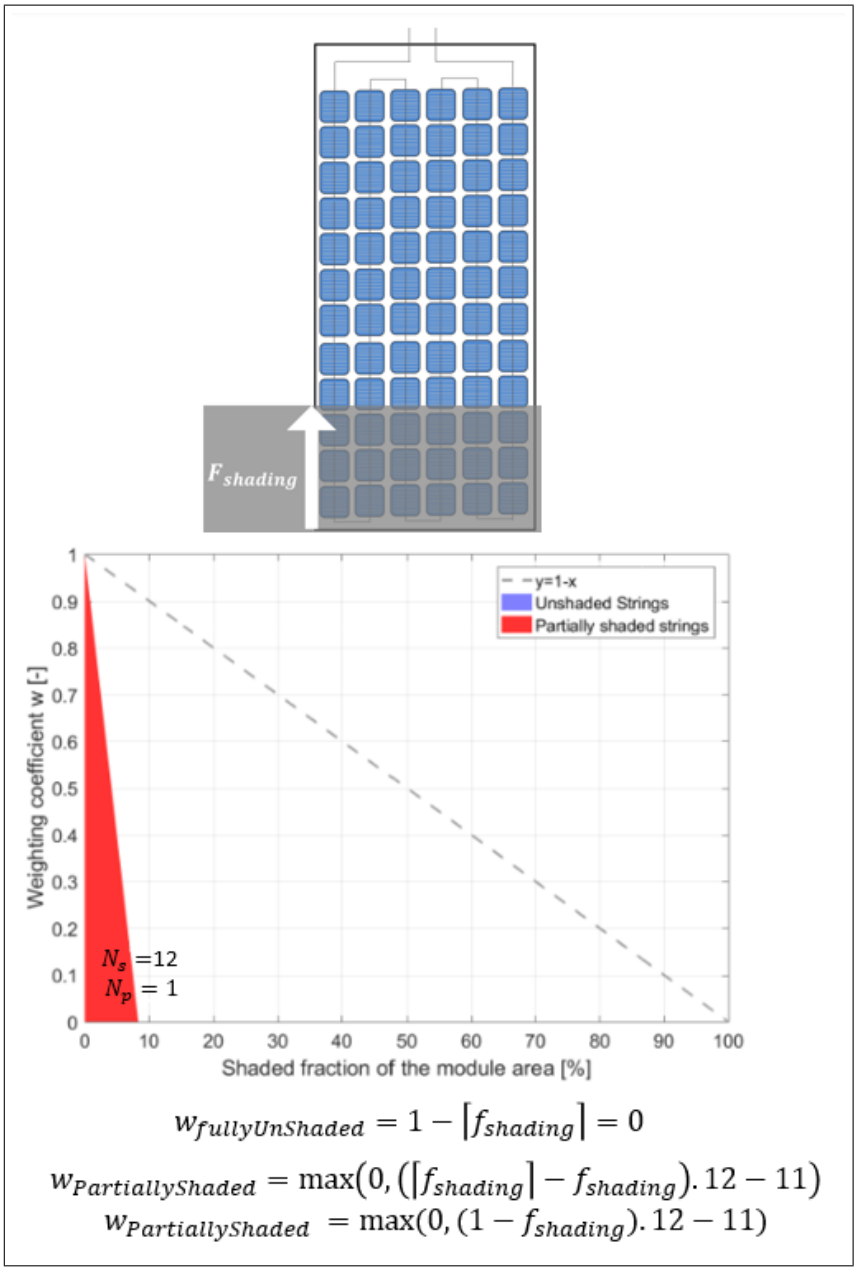

Figure 18: Example of N_s and N_p, $w_{FullyShaded}$ and $w_{PartiallyShaded}$ computation for a 6x12-cells panel in portrait orientation

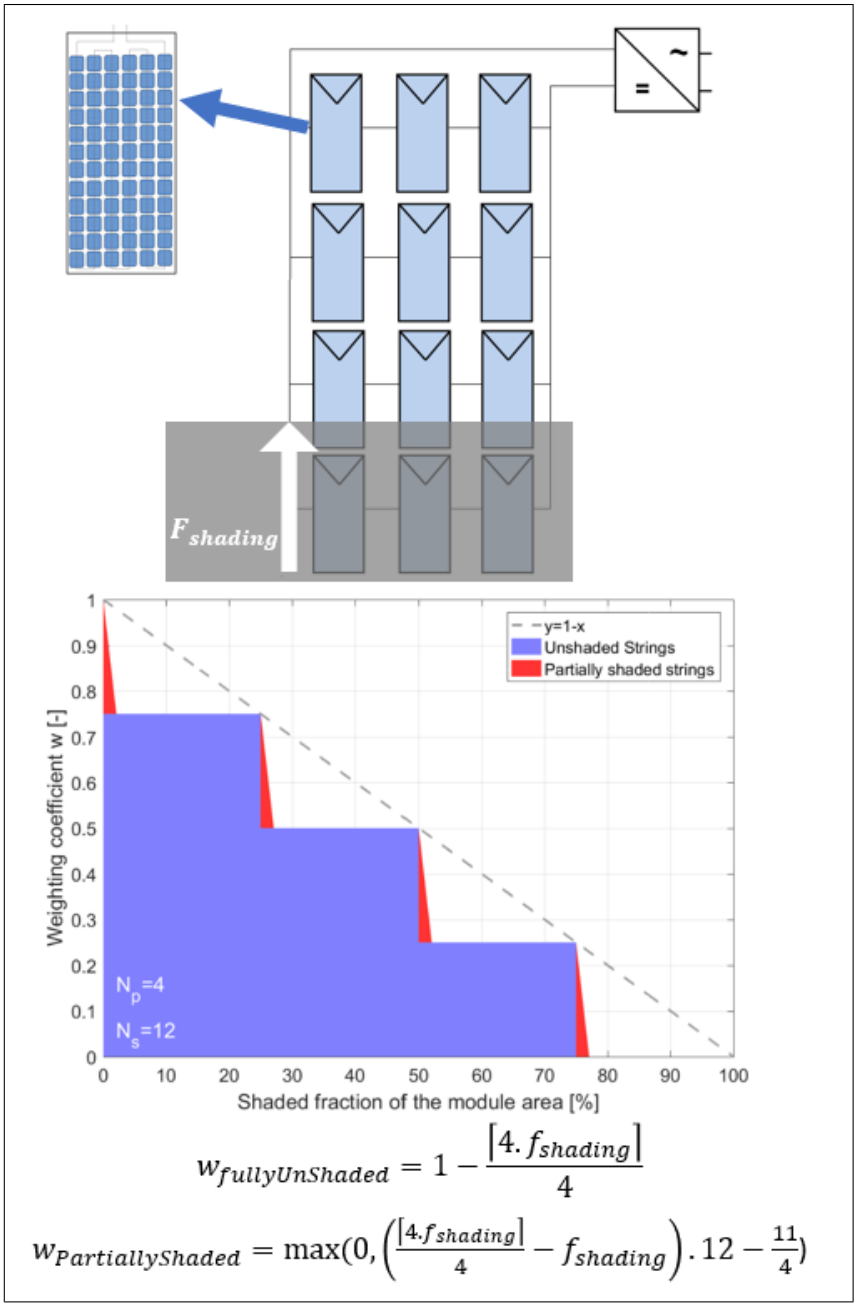

$$w_{fullyUnShaded} = 1 - \frac{\lceil 4.f_{shading} \rceil}{4}$$

$$w_{PartiallyShaded} = \max\left(0, \left(\frac{\lceil 4.f_{shading} \rceil}{4} - f_{shading}\right).12 - \frac{11}{4}\right)$$

Figure 19: Example of N_s and N_p, $w_{FullyShaded}$ and $w_{PartiallyShaded}$ computation for a row of 6x12-cells panels in portrait orientation. The panel connection are 3 in series and 4 in parallel.